JOURNAL OF MATERIALS SCIENCE 27 (1992) 2205–2210

Ductile phase toughening and R-curve behaviour in a B_4C–Al cermet

A. K. BHATTACHARYA, J. J. PETROVIC
Materials Science and Technology Division, Los Alamos National Laboratory, Los Alamos, NM 87545, USA

The R-curve behaviour of a B_4C–Al cermet was studied experimentally using the indentation/strength technique. Microstructural observations clearly indicate that the dominant mechanism contributing towards increasing toughness with crack length is due to bridging of ductile Al phases. It is inferred that ductile toughening, along with toughening due to residual stresses generated upon cooling of the cermet, contribute to this toughening behaviour. Close agreement between experimental results and a simple model is also established.

1. Introduction

Extensive research has been devoted during the last decade to studying the various mechanisms of toughening brittle materials, particularly ceramics and intermetallics. It is now well established that these brittle materials can be considerably toughened using ductile reinforcements [1–7] among others. The ductile particles can be used to increase the toughness, primarily by forming crack-bridging zones. The crack-tip stress intensity is reduced due to the tractions produced by the bridges in the wake of the crack. Important ductile phase-toughened systems that have been studied are cermets of Al_2O_3–Al [1], glass–Al [3], WC–Co [6], B_4C–Al [7] and intermetallic–metal composite γ-TiAl/Ni [4].

Although the primary mechanism for the increase in toughness in these systems, compared to the untoughened matrix, is due to bridging by intact deforming ligaments of the ductile phase, crack deflection by the reinforcement/matrix interfaces also contributes to such enhancement of toughness. Due to these crack-shielding processes, it is expected that these systems could show considerable R-curve behaviour. Although most of the aforementioned work deals with the deformation aspect of the ductile phase and its contribution to the maximum toughness, very few direct studies of R-curve behaviour in a ductile phase-toughened system exist in the literature [4].

Rising R-curve behaviour has been demonstrated in a variety of toughened brittle materials, and various types of mechanism have been proposed depending on the particular system considered. The important mechanisms proposed so far include crack deflection, whisker pull-out, whisker bridging, grain-boundary deflection, microcracking, transformation toughening and ductile phase toughening. Among all these controlling mechanisms, the ductile phase toughening is the least understood. Although various recent theoretical attempts have been made towards understanding the deformation of bridging ductile phases [2, 5, 8], experimental verification of crack propagation behaviour in such materials is very limited. The purpose of the present work is to make experimental observations of R-curve behaviour in B_4C–Al cermet, and to examine the applicability of present theories for describing ductile phase toughening in such materials.

For experimental determination of rising R-curve behaviour in brittle materials, researchers have adopted various techniques. Among these techniques, the compliance method [4, 9, 10], indentation method [11] and indentation/bend technique [12–15] are most often used. In these methods the compliance technique using a CT/notch specimen is the most accurate, but is quite tedious in terms of experimental procedure and the equipment used. Although direct indentation measurement is simple to use, it has primarily demonstrated its usefulness in monolithic materials where the related fracture mechanics concept has been well established. However it has recently been shown [11] that this technique considerably underestimates the fracture toughness in TiN/ZrO_2 composites when compared to other techniques. The indentation/bend technique has been successfully used [13, 14] to study R-curve behaviour in alumina and transformation-toughened PSZ. In the present investigation we have adopted this technique and power law R-curve representation for studying the enhanced toughness behaviour of B_4C–Al composites.

2. Experimental procedure

The B_4C–Al cermets were made by a liquid infiltration method [7]. Porous B_4C compacts made by slip casting and sintering were infiltrated with molten aluminium at 1200 °C for ~ 15–60 min, thus forming B_4C–Al composites. The microstructural and interfacial characteristics were controlled through proper heat treatment of the B_4C. The final composite typically displays a bicontinuous microstructure of B_4C and Al phases as shown in Fig. 1. Microstructural

0022–2461

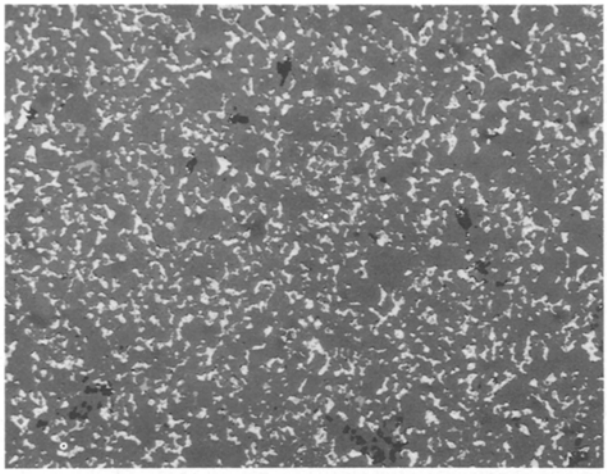

Figure 1 A typical micrograph of the present B_4C–Al cermet containing 12.3 volume fraction of Al phase. Magn. 1000×.

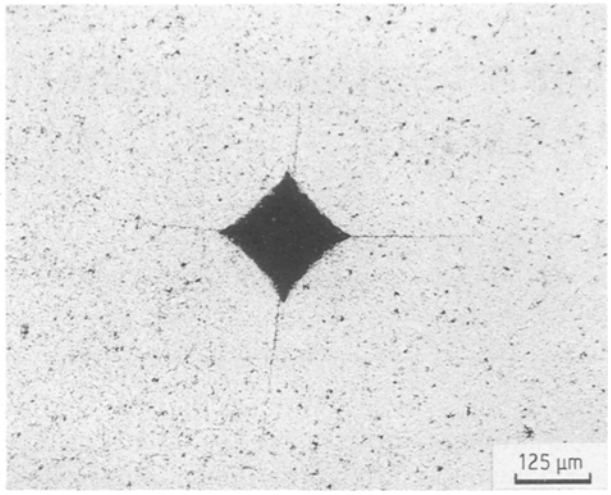

Figure 2 85% B_4C–15% Al diamond pyramid hardness indentation (30 kg load).

analysis indicates the total volume fraction of Al phase to be 12.3%. From the measured Al–B_4C phase boundary surface area per unit test volume, an average Al phase size of 4 μm was estimated. This microstructure also corresponds to a mean free distance of about 5.5 μm for the Al particles.

25 × 5 × 2 mm bars were cut from the as-processed material and polished to a mirror finish on one of the long faces. Three uniform indentation cracks were produced in the centre of the highly polished surface, each 2 mm apart, by Vickers indentation at room temperature. Extreme care was taken so that one set of cracks was produced in such an orientation as to be perpendicular to the tensile stress direction in bending. Various radial flaw sizes were produced this way by indentation loads ranging from 50 to 500 N. No extended lateral flaws were observed other than some small ones localized around the indentation zones. All indentations were made with a speed of 15 s to produce full load and having a hold time of 20 s, after which the specimens were unloaded.

After the indentations were made, the crack lengths in the prospective bending fracture direction were measured by optical microscopy. These crack length values were also compared with the observed crack lengths from *in situ* indentation measurements. A typical micrograph of an indentation with generated cracks is shown in Fig. 2. All indented bars were then tested in a four-point bending fixture with an inner span of 9.5 mm and outer span of 19 mm. The specimens were loaded in such a way that the three serial indentations were subject to tensile loading which was generated by an Instron testing machine at a constant crosshead speed of 0.05 mm min^{-1}. All specimens broke with cracks extending from one of the indentation cracks, and the breaking loads were monitored on a strip-chart recorder.

3. Results and discussion

The indentation/strength procedure for measuring R-curve behaviour has been described in detail in [12–15] and the procedure now seems to be well established. For brevity, only the main steps are outlined here. Firstly an analytical power-law representation is made relating the fracture resistance K_R with crack extension Δa as

$$K_R = k(\Delta a)^m \tag{1}$$

where m is a constant reflecting the extent of R-curve behaviour for the material and k is a constant signifying the level of fracture resistance without the presence of any extra toughening in the material. By relating the fracture mechanics analysis of indentation crack and the applied bending stress, the fracture stress in bending, S, can be related to the indentation load, P, causing the initial control crack as follows:

$$S = \alpha P^{-\beta} \tag{2}$$

where

$$\beta = \frac{(1 - 2m)}{(3 + 2m)} \tag{3}$$

$$\alpha = \frac{k(\beta\gamma)^{\beta}}{Y(1 + \beta)^{1+\beta}} \tag{4}$$

In Equation 4, Y is a dimensionless configuration coefficient which has been adequately described [13] and γ is a constant defined as

$$\gamma = \frac{P}{(a_i)^{\frac{2}{1+\beta}}} \tag{5}$$

where a_i is the initial crack length caused by indentation fracture under a load P. For the purpose of estimating Y and the crack extension Δa in Equation 1, the ratio of crack length a_t at the onset of instability to the initial crack length a_i is also utilized and is given as

$$\frac{a_t}{a_i} = \left(\frac{4}{1 - 2m}\right)^{\frac{2}{3+2m}} \tag{6}$$

For the purpose of controlling the indentation experiments, it is important to note that as given by Equations 1 and 6 the indentation–bend stress tests are

valid for the range of crack lengths where $d \log K_R / d \log(\Delta a) < 0.5$.

First of all the logarithmic plot of Equation 1 is shown in Fig. 3 from which the constants α and β are calculated by linear least-square fit of the data. The coefficient γ was calculated from Equation 5 where the initial crack length is assumed to be the same as the initial crack depth. Table I gives the values of the exponent of crack extention m calculated from Equation 3 and the values of k calculated by using Equation 4 along with other relevant calculated values. The resulting R-curve for this ductile phase-toughened ceramic is shown in Fig. 4, which clearly illustrates the strong R-curve behaviour for this material. For crack extensions from 245 to 1394 μm, the fracture toughness increased from 4.98 to 6.93 Mpa $m^{1/2}$. This is a substantial increase and the underlying dominant mechanism is believed to be ductile phase toughening.

Fig. 5 is a micrograph showing an extended crack which encounters ductile aluminium particles on its propagating path. Fig. 6 illustrates SEM observations of some of these locally stretched aluminium particles bridging the propagating crack near the tip region. This also reveals that the crack propagation path is continuously bridging the aluminium particles confirming a ductile toughening mechanism. No clear indication of any substantial crack deflection was observed for this material. Fig. 7 shows SEM observation of a typical fracture surface after the material was broken in a bending test. A small number of dimples on the fracture surface was observed which is a characteristic of ductile failure for the aluminium particles, but the major mode of final failure seems to be in the form of grain-boundary fracture.

The results obtained in the present investigation are approximate, for the obvious reason that only one specimen was used at each indentation load and thus the absolute fracture toughness values are subject to some uncertainties. Nevertheless, the overall trend of the R-curve is not expected to be substantially altered by increasing the number of experiments, and the present R-curve values are expected to be valid to within a scaling factor. The intention in this work has been to establish the nature of ductile phase toughening in this cermet which effectively gives rise to a pronounced R-curve behaviour.

We now discuss the effects of two toughening mechanisms which are important for this material: (i) toughening due to crack bridging by aluminium particles; and (ii) toughening due to thermal residual stress. From SEM observation of fracture surfaces, it appears that some grain boundary effects are also present. This effect has not been considered in the present analysis and should also be taken into account. Here we examine the above two effects in the light of some of the relevant simple models that have been described in the literature [2, 4, 16].

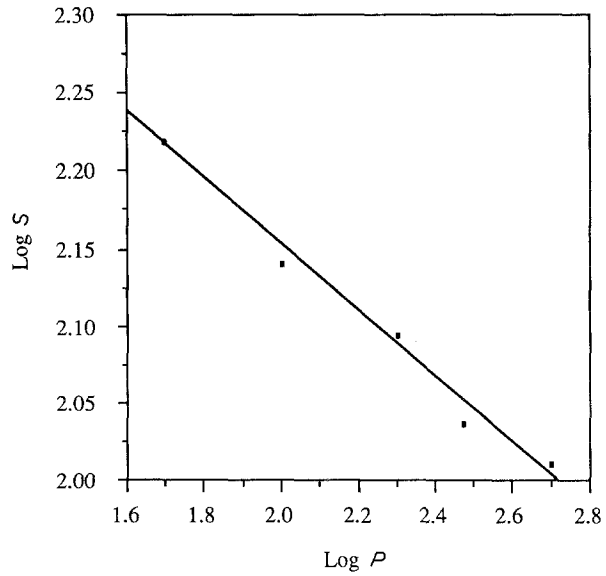

Figure 3 Logarithmic plot of bending strength as a function of indentation load for B_4C–Al cermet. The solid line is a linear least-square fit through the experimental data.

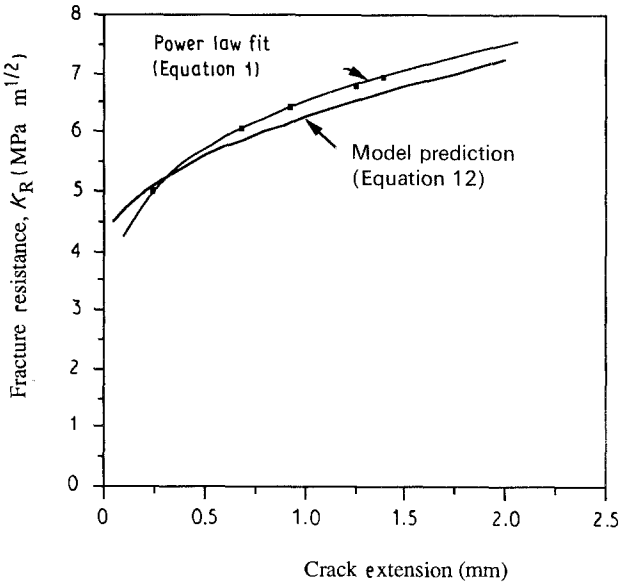

Figure 4 Fracture resistance plotted as a function of crack extension. A power law has been fitted through the experimental data. The results are also compared with the model prediction (■) Experimental data.

3.1. Ductile phase-crack bridging

Ashby *et al.* [2] analysed the toughness enhancement in a ductile, phase-toughened, stiff, brittle matrix by considering the ductile phase to be highly constrained and bonded to the matrix to a various degree. The toughness contribution in this situation is given as

$$\Delta K_{DT} = E\sqrt{Cv_f \frac{\sigma_0}{E} a_0} \quad (7)$$

where E is the inclusion modulus; σ_0 is the initial yield

TABLE I Parameters defining fracture resistance, K_R

Parameter	β	$\log \alpha$	$\log \gamma$	a_t/a_i	Y	m	k
Value	0.182	2.548	8.09	3.03	1.17	0.19	24.16

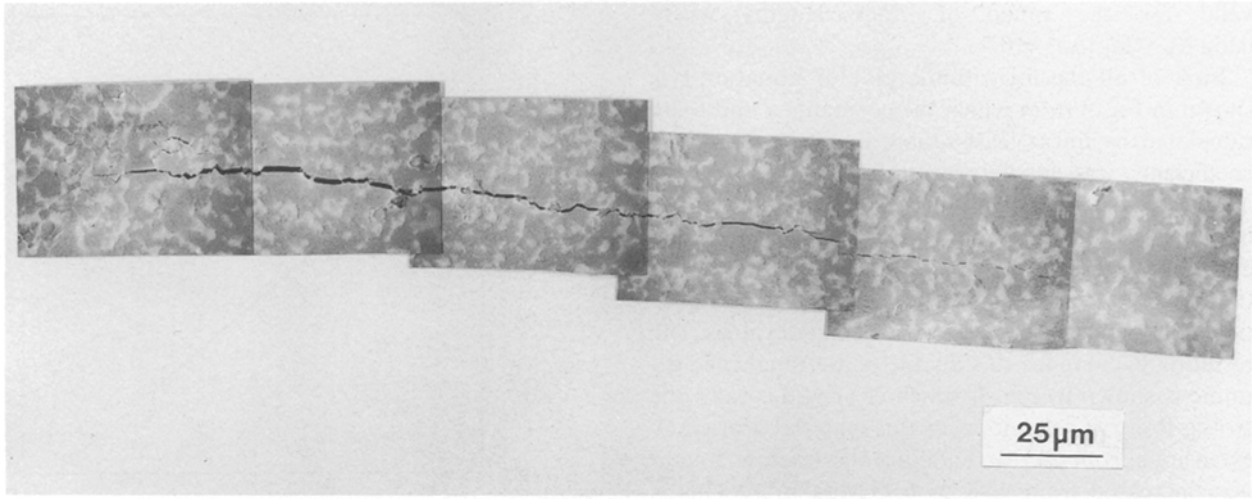

Figure 5 Crack bridging in 85% B_4C–15% Al cermet. The crack has been initiated from 30 kg load indentation.

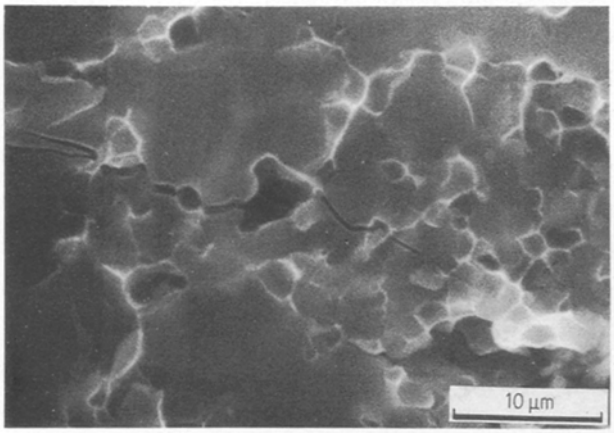

Figure 6 SEM micrograph of a propagating crack front which encounters Al particles. Note that the crack tip has been blocked by ductile particles.

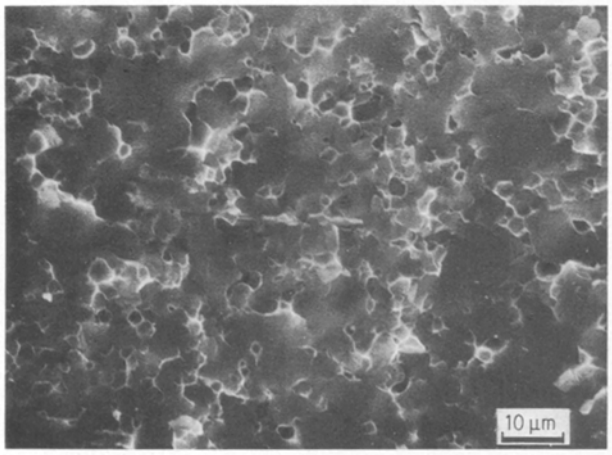

Figure 7 A typical fracture surface after the specimen was broken in a bending test. Note the intergranular nature of the fracture signifying a possible grain-bridging phenomenon along with ductile toughening, as evident in Fig. 6.

strength of the ductile phase; v_f is the area fraction of the ductile phase intersected by the crack; C is a constraint factor ranging from 1.6 for complete bonding with no matrix fracture to 6 for limited bonding or

TABLE 2 Basic material properties for the B_4C cermet

Property	Value
Initial yield strength for the Al Particles, σ_0	150 MPa
Volume fraction of Al particles, f_p	0.123
Average Al particle diameter, $2a_0$	4.5 μm
Mean free distance for Al particles, ϕ	5.5 μm
Young's modulus, E	68.9 GPa
Fracture toughness of B_4C	3.75 MPa $m^{1/2}$

matrix fracture; and a_0 is the particle radius. There is some uncertainty in the evaluation of σ_0 for the ductile particles in this material, as the exact composition of the aluminium particles is not known. However, as various binary and ternary phases in Al–C and Al–B–C have been identified in this cermet [7], we will assume as an approximation that the aluminium particles have 1 wt % of carbon. This gives a value of $\sigma_0 = 150$ MPa [17]. The yield stress value will be higher with higher carbon content in aluminium. We also assume an average constraint factor of 2.25 for the aluminium particles, and utilize the material properties listed in Table II for our calculation. As calculated from Equation 7, this results in an increase of 2.4 MPa $m^{1/2}$ in steady-state toughness value due to ductile bridging in this material.

In studying the fracture process in a Nb-toughened TiAl matrix, Elliott *et al.*, [4] used the representation of crack-tip shielding due to stresses acting on the bridges. From microscopic observation of indentation cracks at various loads in the present investigation, it was seen that the bridge length varied between ~ 40 and 60% of the crack length. For an estimate of the increase in toughness due to crack bridging, we assume that the bridge length is 50% of the crack length on average. This gives rise to the increase in toughness as a function of crack length a as

$$\Delta K_{DT} = 1.9 f_p \sigma_{eff} \sqrt{\lambda a} \quad (8)$$

where f_p is the volume fraction of the particles; a is the crack length; σ_{eff} is the weighted engineering stress in the bridging particles; and λ is the average ratio of bridge length to crack length. Considering an average constraint factor of 2.25 and using particle properties as described earlier, we obtain

$$\Delta K_{DT} = 73\sqrt{a}\,\text{MPa}\sqrt{m} \quad (9)$$

3.2. Thermal residual stress

It is expected that the residual compressive stresses in the matrix, induced by the mismatch in the coefficients of thermal expansion of the matrix and the particles when the composite is cooled down from the processing temperature T_p of 1200 °C to room temperature T_0 will give rise to some toughening. The increase in toughness due to such residual stress can be found as [16]

$$\Delta K_{RS} = 2q\sqrt{\frac{2(\phi - 2a_0)}{\pi}} \quad (10)$$

where q is the average compressive stress in the matrix, ϕ is the interparticle distance. Considering average values of coefficients of thermal expansion in the matrix, α_m, and the particles, α_p, q is given as [16]

$$q = \frac{2f_pE_p\left(\frac{1+v_m}{1-2v_p}\right)(T_0 - T_p)(\alpha_p - \alpha_m)}{(1-f_p)(1+v_m)\left\{2 + \frac{E_p}{E_m}\left(\frac{1+v_m}{1-2v_p}\right)\right\} + 3f_p(1-v_m)\frac{E_p}{E_m}\left(\frac{1+v_m}{1-2v_p}\right)} \quad (11)$$

Using the material properties listed in Table I, we obtain $\Delta K_{RS} = 0.2$ MPa m^{-1} from Equations 10 and 11.

We now compare the fracture toughness values obtained in our experiments with these model predictions. The toughness increase due to thermal stresses can be considered to be invariant to the increase in crack or bridge length. Here we note that the fracture toughness for B_4C matrix, without any potent toughening, is 3.75 MPa m$^{1/2}$ [18]. Thus including residual stress toughening along with the steady-state toughness increase due to ductile bridging, as predicted by Equation 7, we obtain a steady state K_{IC} value of 6.35 MPa m$^{1/2}$. This value is in reasonably good agreement with the range of experimental values determined in our study.

Alternatively, considering the two toughening effects predicted by Equations 9 and 10, we obtain an expression for the prediction of K_{IC} as a function of crack length

$$K_{IC} = K_{IC}(B_4C) + \Delta K_{RS} + \Delta K_{DT} \quad (12)$$

The predictions from Equation 12 for the variation of fracture resistance with crack extension are compared with experimental values, and are shown in Fig. 5. The comparison shows that the results based on this model reasonably predict the whole range of the actual R-curve behaviour of this material. A fracture-toughness value of 8.1 MPa m$^{1/2}$ has been determined earlier for this cermet containing 20 vol % Al-phase (D. Milius, University of Washington, personal communication). Some reduction in toughness values obtained in the current investigation is likely to be due to smaller volume fraction (12.3%) of Al phase in the present work. Also, in the present model a ratio of average ligament length to crack length has been assumed based on experimental observations. This is clearly an approximation in terms of the mechanics of inelastic deformation and fracture process of the ductile phases. However, since it has its foundation in the actual experimental observations, the model makes a reasonably close prediction of the experimental fracture toughness values.

4. Conclusions

The indentation/strength technique can be used to determine R-curve behaviour of a B_4C–Al cermet. With the induced plastic deformation of the ductile particles implicitly assumed as a crack retardation force in the analysis, it has been found that this technique is well adapted for a ductile toughened material. It has also been shown that the resulting R-curve behaviour can be reasonably predicted by a simple model.

Acknowledgements

The authors would like to thank Professor Ilhan Aksay, Dr Dave Milius and Professor Mehmet Sarikaya of the University of Washington for supplying the materials. Thanks are also due to Mary Ann Hill of the Los Alamos National Laboratory for microscopy analysis. Support from DARPA is gratefully acknowledge.

References

1. L. S. SIGL, A. G. EVANS, P. MATAGA, R. M. MCMEEKING and B. J. DALGLEISH, *Acta Metall.* **36** (1988) 946.
2. M. F. ASHBY, F. J. BLUNT and M. BANNISTER, *ibid.* **37** (1989) 1847.
3. V. V. KRSTIC, P. S. NICHOLSON and R. G. HOAGLAND, *J. Amer. Ceram. Soc.* **64** (1981) 499.
4. C. K. ELLIOTT, G. R. ODETTE, G. E. LUCAS and J. W. SHECKHERD, *Mater Res. Soc. Symp. Proc.* **120** (1988) 95.
5. A. G. EVANS and R. M. MCMEEKING, *Acta Metall* **34** (1986) 2435.
6. L. S. SIGL and H. E. EXNER, *Metall. Trans.* **18A** (1987) 1299.
7. A. J. PYZIK, I. A. AKSAY and M. SARIKAYA, in "Ceramics Microstructure—1986", Materials Science Research, edited by J. A Pask and A. G. Evans (Plenum, New York, 1987) p. 45.
8. P. A. MATAGA, *Acta Metall.* **37** (1989) 3349.
9. H. HUBNER and W. JILLEK, *J. Mater. Sci.* **12** (1977) 117.
10. R. STEINBRECH, R. KHEHANS and W. SCHAARWACHTER, *ibid.* **18** (1983) 265.
11. M. V. SWAIN, *Materials Forum* **13** (1989) 237.

12. P. CHANTIKUL, G. R. ANSTIS, B. R. LAWN and D. B. MARSHALL, *J. Amer. Ceran. Soc.* **64** (1981) 539.
13. R. F. KRAUSE, *ibid.* **71** (1988) 338.
14. S. SRINIVASAN and R. O. SCATTERGOOD, *J. Mater. Res. Soc.* **5** (1990) 1490.
15. R. F. COOK and D. R. CLARK, *Acta Metall* **36** (1988) 555.
16. M. TAYA, S. HAYASHI, A. S. KOBAYASHI and H. S. YOON, *J. Amer. Ceram Soc.* **73** (1990) 1382.
17. D. C. HALVERSON, A. J. PYZIK and I. A. AKSAY, *Proc. Ceram Engng Sci.* **6** (1985) 736.
18. G. DEWITH, *J. Mater Sci.* **19** (1984) 457.

Received 7 January 1990
and accepted 7 June 1991